This article has been accepted for publication in a future issue of this journal, but has not been fully edited. Content may change prior to final publication. Citation information: DOI 10.1109/JSEN.2015.2476997, IEEE Sensors Journal

A RFID Sensor for Corrosion Monitoring in Concrete

Walter D. Leon-Salas, *Member, IEEE,* and Ceki Halmen

***Abstract*—A radio frequency identification (RFID) sensor for corrosion monitoring in concrete is presented. The sensor can perform linear polarization, open circuit potential and temperature measurements. The sensor obtains its power from an external RFID reader, which also functions as a datalogger. The sensor's electronic circuit comprises a RFID modem, a low-power microcontroller and a three-electrode low-power potentionstat. The electronic circuit and the three electrodes are housed in a 3D-printed case measuring 11.8 cm×4 cm×5.6 cm. An analysis of the inductive coupling between the reader's and the sensor's antennas is carried out to guide the optimization of the RFID communication link. Tests with a wet and a concrete electrochemical corrosion cells show that the developed sensor has a performance comparable to costly and bulkier benchtop potentiostats. An accelerated corrosion test was conducted by embedding the electrodes in concrete for 24 days. Linear polarization resistance measurements obtained from the developed sensor show the initiation and progression of corrosion. An uncertainty evaluation is carried out showing that the developed RFID sensor has an accuracy compatible with precision benchtop instruments.**

***Index Terms*—RFID, corrosion, concrete, monitoring.**

I. Introduction

CORROSION of concrete reinforcement is one of the main factors leading to premature deterioration of concrete structures worldwide [1]. According to the U.S. Federal Highway Administration (FHWA), the cost of corrosion in the United States is estimated to be around $276 billion per year [2]. The direct cost due to corrosion of highway bridges is estimated to be $8.29 billion, while the indirect costs due to traffic delays and productivity loss is estimated to be much higher [3]. Detecting corrosion in its early stages can inform the scheduling of preventive maintenance measures in order to prolong the service life of the concrete structure and reduce the likelihood of catastrophic failures.

Corrosion monitoring with non-destructive methods are preferable. In particular, the use of wireless concrete-embedded corrosion sensors is appealing since it avoids exposed wires that can themselves corrode or break. Given that most reinforced concrete structures are designed to have a service life of 50 to 100 years, corrosion-monitoring sensors cannot rely on batteries for their power. Instead, passive sensors that harvest their energy from their environment, or from an external reader through inductive coupling, are the most suitable solution.

Several efforts to develop passive embeddable corrosion sensors have been reported in the literature. In [4]–[6] a binary passive sensor based on radio frequency resonance is reported. The sensor consists of an LC tank whose resonant frequency is monitored by an external reader. The LC tank has a steel wire that is exposed to corrosion. As the exposed wire corrodes, it eventually breaks, changing the capacitance of the LC tank and its resonant frequency, which is detected by the external reader. Once the exposed wire breaks, the sensor stops providing new information about the corrosion process.

In [7] a binary passive corrosion sensor dubbed Smart Pebble is reported. The Smart Pebble monitors the potential difference between two electrodes of an electrolytic cell: an ion-selective electrode and a reference electrode. When the potential difference between the electrodes exceeds a threshold, a bit of information is conveyed to an external RFID reader via a RFID tag (MCRF202 from Microchip) by inverting the tag's identification code.

Resonant LC tanks embedded in concrete have been used in [8,9] to monitor the corrosion potential of a steel electrode. The capacitance of the LC tank is set by varactor. The varactor's capacitance varies in response to changes in the corrosion potential, thus changing the resonant frequency of the LC tank. The change in resonant frequency is detected by an external reader. A drawback of this technique is that the corrosion potential is affected by other factors besides corrosion, such as limited diffusion of oxygen, concrete porosity and the presence of highly resistive layers [1]. Hence, monitoring the steel's corrosion potential only provides the likelihood or tendency of corrosion, but not the actual corrosion rate. Another drawback of resonant LC tanks is that the transmission of corrosion information is inherently analog, hence, susceptible to noise.

The effect of eddy currents in the response of RFID tags mounted on corroding steel plates has been investigated in [10]. It was found that the peak amplitude of the RFID tag response is correlated with the atmospheric exposure time of the steel plates. A related work by the same research group presented in [11] showed that the permittivity of corroding steel can be detected using a vector network analyzer and a waveguide.

A well-established technique for determining actual corrosion rates is the linear polarization resistance measurement [12]. Commercially-available sensors such as the Embedded Corrosion instrument (ECi-2) from Virginia Technologies can perform linear polarization resistance readings as well as temperature, resistivity and chloride concentration measurements [13]. The ECi-2 is a digital peripheral instrument on a local area network embedded inside the concrete structure. The network communicates with an external datalogger for corrosion data read-out. Due to the large scale of the embedded local area network, this solution is most suitable for new

W. D. Leon-Salas is with the School of Engineering Technology, Purdue University, West Lafayette, IN, 47907 USA, e-mail: wleonsal@purdue.edu.

Ceki Halmen is with the Department of Civil and Mechanical Engineering, University of Missouri-Kansas City, Kansas City, MO.

This article has been accepted for publication in a future issue of this journal, but has not been fully edited. Content may change prior to final publication. Citation information: DOI 10.1109/JSEN.2015.2476997, IEEE Sensors Journal

construction projects where the sensors can be wired up before the concrete is poured.

In this work we present a RFID-based sensor suitable for corrosion monitoring in reinforced concrete structures. The sensor can perform linear polarization, open circuit potential and temperature measurements. The sensor can also measure its own power supply voltage and relay that information to the external reader, which can then modify its power output accordingly. The sensor obtains its power from an external RFID reader, which also functions as a datalogger. The sensor employs a RFID modem that supports the ISO 15693 and the ISO 18000 communication standards. Hence, commercially-available RFID readers can be employed to communicate with the sensor.

Unlike other wireless corrosion sensors, communication between the sensor and the reader is fully digital and employs cyclic redundancy checks (CRC) and collision detection, guaranteeing that the data read from the sensor is free from transmission errors. Moreover, communication is bidirectional which allows digital commands to be sent to the sensor. This bidirectionality enables the developed sensor to perform several types of measurements, namely, linear polarization, open circuit voltage, temperature and power supply voltage. Temperature sensing comes at no additional hardware cost because the microcontroller employed in the sensor design incorporates an on-chip temperature sensor. The developed corrosion sensor can be installed in new structures before concrete is poured, but it is small enough to be installed in existing concrete structures via a back-filled core. This work is an extension of our work presented in [14]. Here the sensor is fully characterized and tested in both a wet and a concrete electrochemical cell.

The rest of this paper is organized as follows: section II provides a brief overview of the corrosion process in steel, section III describes the sensor design and operation, section IV presents measurements collected with the developed sensor and with a benchtop potentiostat using a wet and a concrete-based electrochemical cell. Section V concludes the paper.

II. Corrosion Overview

A. Corrosion of Reinforcement in Concrete

Corrosion of reinforcing steel in concrete occurs via coupled anodic and cathodic electrochemical reactions at the steel-concrete interface. The anodic and cathodic reactions take place with the help of concrete pore water, which acts as an electrolyte. In the anodic reaction, steel is oxidized releasing electrons, which flow into the steel and iron ions that go into solution. This anodic reaction is expressed as follows:

$$Fe \rightarrow Fe^{+2} + 2e^{-} \tag{1}$$

The cathodic reaction can take different forms depending on the availability of oxygen and the pH of the environment. If oxygen is available and if the concrete is highly alkaline, with a pH in the range of 12.5 to 13.5, water is reduced producing hydroxyl ions as shown in (2):

$$1/2O_2 + H_2O + 2e^{-} \rightarrow 2OH^{-} \tag{2}$$

The product of the anodic and cathodic reactions (iron ions and hydroxyl ions) combine together to produce ferrous hydroxide:

$$Fe^{+2} + 2OH^{-} \rightarrow Fe(OH)_2 \tag{3}$$

Ferrous hydroxide in turn can be further oxidized into products producing a stable film that passivates and protects the reinforcing steel from further corrosion [15]. This passive film, however, can be destroyed and localized corrosion can be initiated. The main mechanisms that destroy the passive film are carbonation and chloride ingression [16,17].

When atmospheric carbon dioxide diffuses into the concrete, it neutralizes the alkalis, reducing the pH of the concrete pore solution. Chloride ions, on the other hand, displace O^{2-} from the passive layer leading to initiation of the passive film destruction [18]. Typical sources of chloride ions are de-icing salts and seawater exposure. The volume of corrosion products can be more than six times larger than the volume of steel [15]. Such volume increase inside hardened concrete causes stresses that lead to cracking, spalling, and serious deterioration of structural concrete. Further, corrosion of reinforcing steel results in a reduction of the steel cross-section, loss of steel ductility, and reduced bond strength between the steel and concrete [19].

B. Corrosion Cell and Linear Polarization

A corrosion cell is a device employed to measure the anodic and cathodic electrochemical reactions of a corroding metal. A typical corrosion cell consists of three electrodes (working, reference and counter electrodes) submerged in an electrolyte. The working electrode (WE) is made out of the corroding metal. The reference electrode (RE) is an electrode with a stable potential that provides a reference for measurements in the cell. Common reference electrode chemistries are silver/silver chloride, saturated calomel and copper/copper sulfate. The counter electrode (CE) works as a current source and is made of a material that does not corrode.

1) Cell Potential: The cell potential, also known as Open-Circuit Potential (OCP), is the potential difference between the WE and the RE. The measurement of the OCP is a common procedure for corrosion inspection of reinforced concrete structures. This technique is described in the ASTM C 876, Standard Test Method for Half-cell Potentials of Uncoated Reinforcing Steel in Concrete. According to this standard, if the OCP, measured using a saturated copper/copper sulfate (CSE) reference electrode, is below -0.350 V, the probability of corrosion is more than 90% [20]. The OCP measurement technique gives only an estimation of the likelihood of corrosion but does not provide information on the actual rate of corrosion.

Further, OCP readings can be below -0.350 V without significant presence of corrosion. If oxygen access is restricted, the steel becomes active but corrosion does not progress and the measured OCP can fall to values of -1 V [18]. Other factors affecting OCP readings are the presence of high resistive layers of concrete, the age of the concrete and the position of the reference electrode [21]–[23]. Hence, OCP

This article has been accepted for publication in a future issue of this journal, but has not been fully edited. Content may change prior to final publication. Citation information: DOI 10.1109/JSEN.2015.2476997, IEEE Sensors Journal

readings alone are not sufficient for a reliable measurement of the corrosion rate of reinforcing steel.

2) Linear Polarization: Linear polarization is an electrochemical technique employed to measure the instantaneous corrosion current, I_{corr}, of the WE and the dynamics of the anodic and cathodic reactions. A popular model that describes the anodic and cathodic reactions is given by the Butler-Volmer equation as follows:

$$I_{cell} = \underbrace{I_{corr} e^{2.3(E_{cell}-E_{OC})/\beta_a}}_{I_{anodic}} - \underbrace{I_{corr} e^{2.3(E_{OC}-E_{cell})/\beta_c}}_{I_{cathodic}} \quad (4)$$

where, I_{cell} is cell current flowing between the CE and the WE, E_{cell} is the potential difference between the WE and the RE, E_{OC} is the OCP, and β_a and β_c are the Tafel constants for the anodic and the cathodic reactions, respectively.

In a linear polarization measurement, the corrosion cell potential E_{cell} is moved away from E_{OC} disrupting the balance between the anodic and cathodic reactions. As E_{cell} changes, the cell's current I_{cell} is measured. Figure 1 shows the anodic and cathodic reactions currents as well as the cell's current I_{cell} as predicted by the Butler-Volmer equation for the case $\beta_a = 2\beta_c$. From the figure, it can be seen that the anodic reaction dominates for $E_{cell} \gg E_{OC}$ (anodic region) while the cathodic reaction dominates for $E_{cell} \ll E_{OC}$ (cathodic region). At $E_{cell} = 0$ both reactions are in equilibrium and the current through the cell is $I_{cell} = 0$.

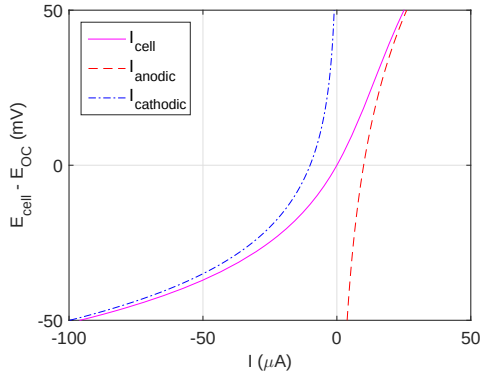

Figure 1. Anodic and cathodic currents of a corroding metal as predicted by the Butler-Volmer equation.

The corrosion current I_{corr} can be estimated from the E_{cell} vs. I_{cell} curve using different approaches. A common approach also taken in this work, involves the calculation of an intermediate parameter known as the polarization resistance R_p. From Figure 1 we see that in the vicinity of the OPC (within 10 to 30 mV) the potential-current curve is fairly linear. The slope of the curve when $E_{cell} = E_{OC}$ is defined as the polarization resistance [24]. From equation (4) the slope of the potential-current curve at $E_{cell} = E_{OC}$ is given by:

$$R_p = \left.\frac{\Delta E_{cell}}{\Delta I_{cell}}\right|_{E_{cell}=E_{OC}} = \frac{\beta_a \beta_c}{2.3 I_{corr}(\beta_a + \beta_c)} \quad (5)$$

From (5) the corrosion current can be solved to obtain:

$$I_{corr} = \frac{1}{2.3 R_p}\left(\frac{\beta_a \beta_c}{\beta_a + \beta_c}\right) = \frac{B}{R_p} \quad (6)$$

where B is a proportionality factor and a function of the Tafel constants β_a and β_c. The Tafel constants can be determined as the slopes of the E_{cell} vs. $\log(I_{cell})$ curve in the anodic and cathodic regions [25]. Once B and R_p are known, the corrosion current is calculated using (6). Of importance in corrosion monitoring is the calculation of thickness reduction of the material per unit time ($\Delta s/\Delta t$). Thickness reduction can be determined from Faraday's equations [26]:

$$\frac{\Delta s}{\Delta t} = 3268\left(\frac{B}{R_p A}\right)\left(\frac{M}{z\rho}\right) \text{ mm/year} \quad (7)$$

where, M is the mol mass of the metal, A is the area of the working electrode, z is the number of electrons in the reaction equation for the anodic reaction (per atom of the dissolving metal) and ρ is the density of the metal.

III. Sensor Design and Operation

Figure 2 shows a conceptual operation diagram of the proposed RFID-based corrosion sensor. For clarity, in the figure the sensor is shown above the reinforcement bar (rebar) but in an actual deployment the sensor and the rebar will be at the same distance from the external surface of the concrete for sensor readings to correlate with the rebar. The concrete structure is naturally exposed to chlorides, oxygen and water which diffuse through concrete and reach the rebar. When chloride ions reach the rebar, the steel's passive film is disrupted leaving steel exposed to corrosion. The presence of oxygen and water start and maintain the corrosion process.

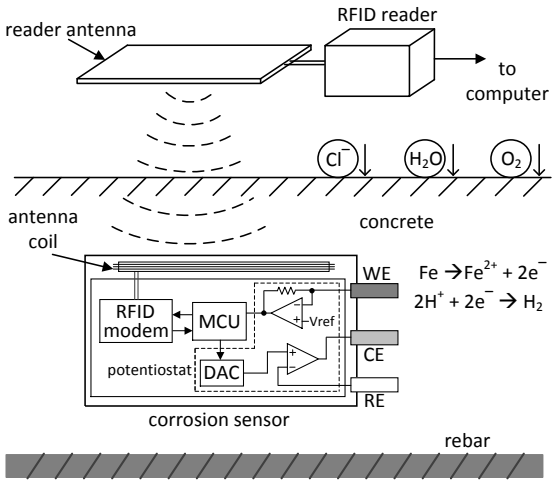

Figure 2. Conceptual diagram of the operation of the proposed RFID-based corrosion sensor.

The sensor incorporates a low-power three-electrode potentiostat, which is used to perform linear polarization measurements. The potentiostat measures the current that flows between WE and the CE while the potential of the CE with respect to the RE is varied. The WE is a piece rebar steel while the CE is made out of a conductive material that does not corrode. Typical materials for the CE are carbon, nickel and stainless steel. In this work a carbon electrode was used. The function of the RE is to provide a stable and known

This article has been accepted for publication in a future issue of this journal, but has not been fully edited. Content may change prior to final publication. Citation information: DOI 10.1109/JSEN.2015.2476997, IEEE Sensors Journal

potential reference. In this work a silver-silver chloride RE was employed. A linear polarization curve is obtained by plotting the CE potential against the WE current. The corrosion state of the WE can be extracted from the polarization curve. When the corrosion sensor is placed in close proximity to a rebar, then the corrosion state of the WE is a good estimation of the corrosion state of the rebar.

Since the corrosion sensor is expected to last as long as the concrete structure, it cannot rely on batteries as its energy source. Battery leakage and the limited number of charge-discharge cycles of batteries will limit the lifetime of the sensor. Instead, the proposed sensor relies on inductive coupling to power itself and for data communications. Inductive coupling is a well established technique employed in RFID systems. The proposed corrosion sensor includes a RFID modem to communicate to commercially-available RFID readers.

The sensor also comprises a low-power micro-controller unit (MCU), which controls the potentiostat and reads linear polarization curves. The polarization curves are stored on an electrically erasable programmable read-only memory (EEPROM). The EEPROM and the RFID modem are integrated in a single chip. The RFID reader accesses the EEPROM contents through the RFID modem and reads the measured linear polarization curve. The data collected by the RFID reader is sent via a serial port to a computer where the polarization curve is analyzed and displayed.

A. Electronic Circuit

Figure 3 shows the schematic circuit of the corrosion sensor. The sensor comprises a low-power mixed-signal MCU (Texas Instruments MSP430F2012), a dual-access EEPROM with integrated RFID modem (ST Microelectronics M24LR64), a 16-bit digital-to-analog converter (Texas Instruments DAC8411) and three micro-power opamps OA_1 and OA_2 (Texas Instruments OPA2369) and the low-offset zero-drift OA_3 (Texas Instruments OPA330).

The MCU has an integrated 8-input 10-bit analog-to-digital converter (ADC), on-chip voltage reference generation, a temperature sensor, I2C and SPI serial protocol support and five power-saving modes. The MCU communicates with the external RFID reader via a RFID modem and a coil antenna. The AC voltage developed at the coil antenna is rectified by the diode bridge and regulated by the low-dropout regulator (LDO) to generate a stable supply of 3.0 V for the sensor. The capacitor C_T is a variable capacitor used to tune the antenna to the RFID carrier frequency of 13.56 MHz. The zener diode Z_1 protects the LDO from excessively large voltages. The choke inductor L_1 blocks the high carrier frequency into the LDO to reduce power supply noise. The role of C_{stab} is to smooth out the voltage rectified by the diode bridge. Resistors R_1 and R_2 form a voltage divider that allows the MCU to monitor the V_{dc} input voltage to the LDO. The V_{dc} voltage can then be read by the external RFID reader which can adjust its output power level accordingly.

The operational amplifiers OA_1 to OA_3, the digital-to-analog converter (DAC) and the switch S_1 constitute a three-electrode potentionstat which is used to perform linear polarization measurements. To carry out a linear polarization

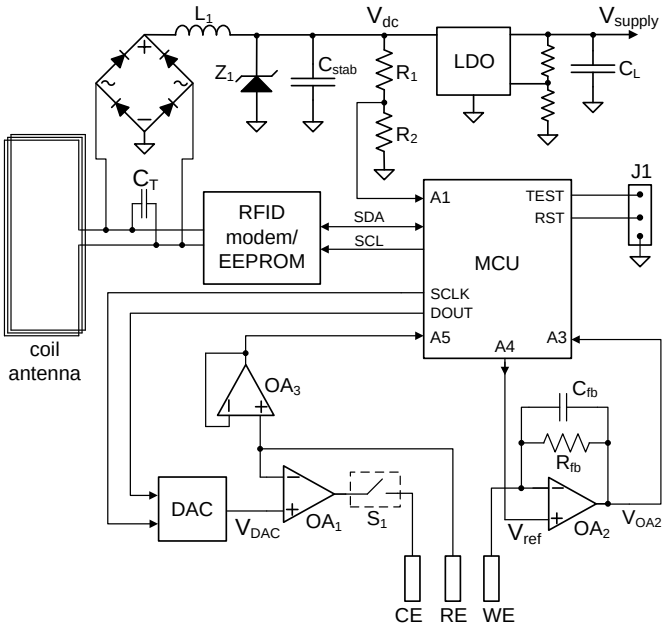

Figure 3. Schematic diagram of the corrosion sensor circuit.

measurement, the Open Circuit Potential (OCP) of the corrosion cell must be measured first. To measure the OCP, the MCU first opens switch S_1 and generates voltage reference $V_{ref} = 1.5$ V (through pin A4). The virtual ground effect of opamp OA_2 sets the WE potential to V_{ref}. The potential of the RE is read through ADC channel A5. Opamp OA_3 in unity-gain buffer configuration isolates the RE from the internal ADC sample-and-hold circuit. The OC voltage is readily computed by subtracting V_{ref} from the measured RE potential.

To perform a linear polarization measurement the MCU closes switch S_1, outputs voltage reference V_{ref} and programs the DAC to output the following voltage:

$$V_{DAC} = \begin{cases} \text{OCP} - 20 \text{ mV} & \text{if } \textit{ramp} = \text{up} \\ \text{OCP} + 20 \text{ mV} & \text{if } \textit{ramp} = \text{down} \end{cases} \quad (8)$$

The variable *ramp* controls the direction of the linear polarization measurement. If *ramp* = up, V_{DAC} is increased from OCP $-$ 20 mV to OCP $+$ 20 mV. If *ramp* = down, V_{DAC} is decreased from OCP $+$ 20 mV to OCP $-$ 20 mV. The ramp's rate of increment and the number of points can also be changed by the user through the RFID interface. For each point in the ramp, the output of opamp OA_2, V_{OA2}, is read by the MCU using its internal ADC. The current through the WE, I_{cell}, is measured by reading the voltage generated as I_{cell} flows through R_{fb}. Equation (9) shows this relationship:

$$I_{cell} = \frac{V_{OA2} - V_{ref}}{R_{fb}} \quad (9)$$

The function of capacitor C_{fb} (in parallel with R_{fb}) is to filter out high-frequency noise from the linear polarization readings. To reduce noise in the readings even further, every point in the polarization curve is read 64 times and the average is reported. The same approach is followed when measuring the OCP.

This article has been accepted for publication in a future issue of this journal, but has not been fully edited. Content may change prior to final publication. Citation information: DOI 10.1109/JSEN.2015.2476997, IEEE Sensors Journal

B. RFID Communications

The component that enables RFID communications is the dual-interface EEPROM. This EEPROM has an integrated RFID modem that operates at a frequency of 13.56 MHz and supports the ISO 15693 and ISO 18000 RFID communication standards. Therefore, a commercially-available RFID reader can be employed to read and write the content of the EEPROM. The EEPROM can also be accessed via an I2C port. Using the I2C port the MCU can read and write the EEPROM contents. Hence, the external RFID reader and the MCU can exchange data by reading and writing to specific locations of the dual-interface EEPROM.

To send a command to the MCU, the RFID reader writes a byte in the EEPROM location 0000h. Every second the MCU reads location 0000h. If a new command has been written, the MCU proceeds to execute it. When command execution is finished, the MCU asserts the IDLE bit (bit 3 of location 0000h) to signal the reader that the command has been executed. When the MCU is not executing a command, it goes into a low-power mode (LPM3) to reduce power consumption.

The commands that the MCU can execute include performing a linear polarization measurement, reading the OCP, reading temperature and reading the supply voltage V_{dc}. The measurement results are stored in pre-defined memory locations which can then be read by the RFID reader. The RFID reader reads the polarization curve in blocks of 32 bytes each. Each block of data has a CRC and a collision data field. If the CRC check fails or if a collision is detected, the data block is read again until the CRC check is correct and no collisions are detected. This error detection mechanism ensures that data from the sensor is free from transmission errors.

C. Power Consumption

The current consumption of the different components of the corrosion sensor were measured. The sensor consumes on average 100.2 μA when it is in the idle state waiting for a command from the external reader. The highest average current consumption is 225.2 μA and occurs when the sensor is performing a linear polarization measurement.

Table I shows the current consumption of individual components of the corrosion sensor as a percentage of the total current. The highest current consumption occurs when the reference voltage generation circuit is turned on and its output routed outside the MCU. Using a discrete reference voltage generation circuit (outside the MCU) could further reduce the current consumption of the sensor.

Table I
MEASURED PERCENTAGE CURRENT CONSUMPTION OF THE DIFFERENT COMPONENTS OF THE CORROSION SENSOR.

Component	Consumption
OPA330	18 %
OPA2369	9 %
DAC	22 %
ADC + Vref	38 %
MCU	7 %
RFID EEPROM	6 %

Figure 4 shows the measured instantaneous current consumption of the sensor while it is idle, reading the OCP and performing a linear polarization measurement. The large current peaks are due to the reference circuit being turned on and off. To reduce the average current consumption, the reference circuit is turned on just before a voltage reading takes place.

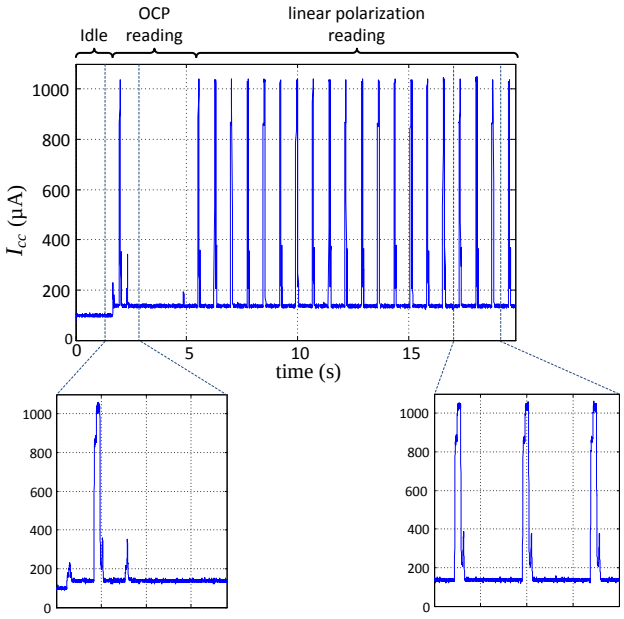

Figure 4. Measured current consumption of sensor during an OCP and linear polarization reading.

D. Inductive Coupling Analysis

In this section an analysis of the inductive coupling link between the sensor and the RFID reader is carried out. The analysis results in a model that will then be used to guide the optimization of the inductive coupling link. The inductive coupling link analysis will follow the approach presented in [27]. Figure 5 shows the circuit modeling the inductive coupling between the sensor and the RFID reader.

The reader's antenna is modeled with inductor L_1. R_{s1} models the resistance of L_1 in series with the output resistance of the voltage source v_p. Likewise, the coil antenna of the sensor is modeled with the inductor L_2 with series resistance R_{s2}. The capacitor C_2 models the capacitances in parallel with the sensor's antenna which includes the tuning capacitor and the input capacitance of the RFID modem.

The load resistance R_{load} models the current consumption of the sensor's circuitry. The antennas of the reader and the sensor constitute two mutually coupled coils with mutual inductance M. The series resistance of the linear regulator (LDO) and the load resistance can be modeled with a single D.C load R_{dc}.

The value of R_{dc} is given by the following equation [27]:

$$R_{dc} = \begin{cases} R_{load} & \text{if } V_{dc} < V_{supply} \\ R_{load}\left(\frac{V_{dc}}{V_{supply}}\right) & \text{if } V_{dc} \geq V_{supply} \end{cases} \quad (10)$$

The full-wave rectifier and the DC load R_{dc} can in turn be modeled by an equivalent AC load R_{ac}. It can be shown that

This article has been accepted for publication in a future issue of this journal, but has not been fully edited. Content may change prior to final publication. Citation information: DOI 10.1109/JSEN.2015.2476997, IEEE Sensors Journal

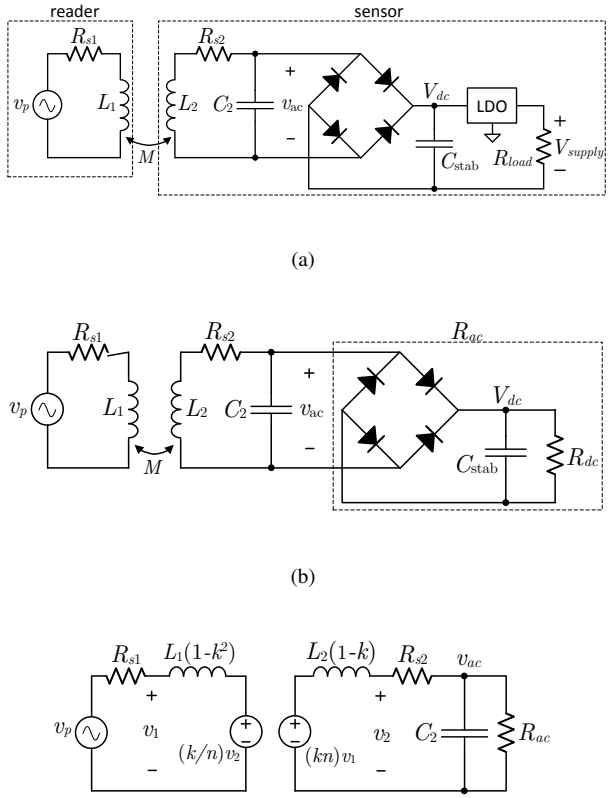

Figure 5. Equivalent circuits: (a) circuit modeling the inductive coupling between the corrosion sensor and the RFID reader; (b) circuit showing the equivalent AC load produced by the combination of the full-wave rectifier and the DC load R_{dc}; (c) equivalent circuit with non-coupled inductors.

the value of the equivalent AC load R_{ac} is given by [27]:

$$R_{ac} = \frac{R_{dc}}{2}\left(1 + \frac{2V_{diode}}{V_{dc}}\right) \tag{11}$$

where V_{diode} is the voltage drop across the diodes in the voltage rectifier bridge. Replacing (10) in (11) yields:

$$R_{ac} = \frac{R_{load}}{V_{supply}}\left(\frac{V_{dc}}{2} + V_{diode}\right) \tag{12}$$

To simplify the analysis of the circuit in Figure 5(b), the mutually-coupled inductors are replaced with the non-coupled inductors $L_1(1-k^2)$ and $L_2(1-k)$ and with two voltage-dependent voltage sources as shown in Figure 5(c).

From the equivalent circuit in Figure 5(c) the following expressions for v_1 and v_2 can be written:

$$v_1 = \frac{k}{n}v_2 + j\omega L_1(1-k^2)\left(\frac{v_p - (k/n)v_2}{R_{s1} + j\omega L_1(1-k^2)}\right) \tag{13}$$

$$v_2 = knv_1\left(\frac{Z_2}{Z_2 + R_{s2} + j\omega L_2(1-k)}\right) \tag{14}$$

where k is the coupling coefficient between the antennas and is given by:

$$k = \frac{M}{\sqrt{L_1 L_2}} \tag{15}$$

and

$$n = \sqrt{\frac{L_2}{L_1}} \tag{16}$$

Given a value of v_p equations (13) and (14) can be solved iteratively using the procedure outlined in Listing 1. In the listing, i is the iteration number. The values of v_1 and v_2 converge in less than 50 iterations.

```
1) i = 0
2) Set v2[i] = Vload + 2Vdiode
3) Rac[i] = Rload
4) Vdc[i] = Vload
5) Use (13) and v2[i] to find v1[i]
6) Use (14) and v1[i] to find v2[i+1]
7) Update Rdc according to (10)
8) Update Rac according to (12)
9) Set Vdc[i+1] = v2[i+1] − 2Vdiode
10) i = i + 1
11) If i > 50 end
12) Go to 5)
```

Listing 1. Iterative procedure to find the values of v_1 and v_2

To validate the model, V_{dc} was measured for different values of the reader's output voltage v_p. In the measurements, the reader and the sensor coil antennas were separated by a concrete block of a thickness of 3 cm. The coupling coefficient k of the measurement setup was estimated using the procedure described in section IV-A and was found to be 0.762. Figure 6 shows the measured values of V_{dc} and the values predicted by the model for $L_1 = 400$ nH, $L_2 = 3.9$ μH, $C_2 = 35$ pF, $R_{load} = 20$ kΩ, $R_{s1} = 50.8$ Ω, $R_{s2} = 0.5$ Ω, $V_{load} = 3.0$ V and $\omega = 2\pi \times 13.56 \times 10^6$. Notably, the measurements and the model agree fairly well and show that to obtain a V_{dc} voltage of 3.1 V or more (the LDO dropout voltage is about 0.1 V), the amplitude of v_p should be at least 4.4 V_{pp}. For a different concrete thickness, the coupling coefficient can be measured again and the model used to calculate the minimum output voltage of reader.

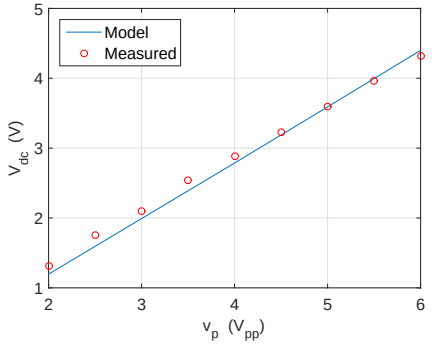

Figure 6. Measured and modeled values of V_{dc} as the reader's output voltage v_p is varied.

This article has been accepted for publication in a future issue of this journal, but has not been fully edited. Content may change prior to final publication. Citation information: DOI 10.1109/JSEN.2015.2476997, IEEE Sensors Journal

E. Sensor Board and Sensor Assembly

A printed circuit board (PCB) hosting the electronic components of the sensor was designed and fabricated. Figure 7 shows the PCB with the mounted components. The PCB size (including mounted components) is 5 cm×3 cm×1.8 cm. The PCB includes a three-pin connector to attach the three electrodes to the board.

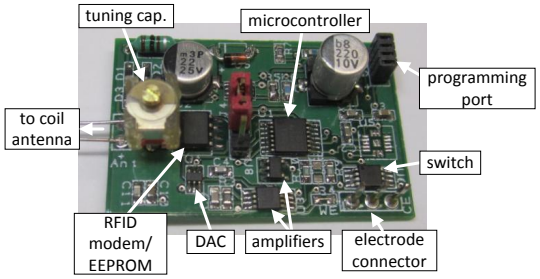

Figure 7. Populated printed circuit board of the corrosion sensor.

The WE was manufactured from a piece of rebar. The rebar piece was machined to create a working electrode of dimensions 1.3×0.5×1.0 cm^3. A wire was attached to the working electrode using conductive epoxy. The CE was implemented using a carbon electrode of dimensions 1.5×0.5×1.5 cm^3. The RE is a rugged silver/silver chloride electrode fabricated by Cathodic Protection Co. and especially designed to be embedded in concrete [28]. The electrode element of the RE is a 99.9% pure silver wire and the electrode media is a specially formulated Ag/AgCl matrix. The electrode is encased in a PVC tube with a cementitous based end plug.

A support structure for the PCB, the electrodes and antenna was designed and fabricated using 3D printing. Figure 8 shows the 3D printed structure with the different components of the corrosion sensor. The working and counter electrodes are positioned facing each to create a direct current flow path. The surface of the working electrode not facing the counter electrode was coated with epoxy to avoid non-direct current contributions. The exposed area on the working electrode is 0.55 cm^2. The sensor's antenna was fabricated by winding 28 AWG magnet wire around a 3D printed support structure with a groove to guide the wire. The inductance of the sensor antenna was measured to be 3.9 μH.

Figure 8(b) shows the assembled sensor along with a cover designed to protect the sensor from the environment. The cover's inside is coated with ferrite sheet to isolate the sensor electronics from the field radiated by the RFID reader minimizing induced noise. A two-part epoxy was used to fix the electrodes to their final positions. The electrodes connect to the PCB via a three-pin connector. The dimensions of the fully assembled sensor are 11.8 cm×4 cm×5.6 cm.

IV. Results and Measurements

The corrosion sensor system was characterized in the laboratory under different conditions. A procedure to measure the coupling coefficient k of the coupled reader-sensor antenna system was performed first. In a second test, linear polarization measurements were performed on a wet electrochemical

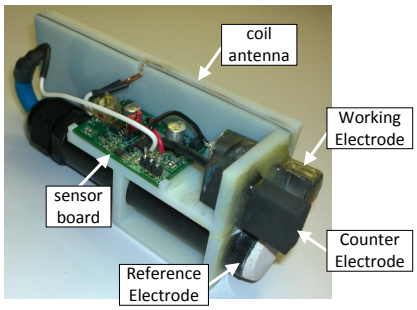

(a)

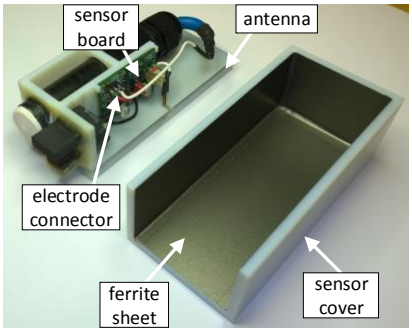

(b)

Figure 8. Assembly of corrosion sensor using 3D printed support structures: (a) sensor board with antenna and electrodes; (b) sensor assembly with cover coated with ferrite sheet.

corrosion cell using the corrosion sensor and a benchtop potentiostat. Finally, in an accelerated test the electrodes were embedded in concrete and corrosion was monitored for several days.

A. Coupling Coefficient Measurement

To measure the coupling coefficient k, the reader and the sensor antennas were placed facing each other on opposite sides of a concrete block of 3 cm thickness. The reader antenna was connected to a function generator while the sensor antenna was connected to an oscilloscope.

The function generator was set to generate a sinusoid of frequency 13.56 MHz and amplitude $U_1 = 1$ V. The amplitude, U_2, of the voltage induced at the sensor antenna was measured with an oscilloscope. The coupling coefficient was then be calculated as follows [29]:

$$k = \gamma \, \frac{U_2}{U_1} \sqrt{\frac{L_1}{L_2}} \tag{17}$$

where γ is a correction factor that accounts for the parasitic capacitance of the oscilloscope probe C_{probe} and is given by [29]:

$$\gamma = 2 - \frac{1}{1 - \omega^2 C_{probe} L_2} \tag{18}$$

Using equations (17) and (18), $C_{probe} = 10$ pF and a measured value of $U_2 = 2.87$ V yields a coupling coefficient value of $k = 0.762$. This coupling coefficient value indicates a strong coupling between the antennas due in part to the

This article has been accepted for publication in a future issue of this journal, but has not been fully edited. Content may change prior to final publication. Citation information: DOI 10.1109/JSEN.2015.2476997, IEEE Sensors Journal

relatively large size of the antennas (12 cm $\times$ 12 cm for the reader antenna and 4 cm $\times$ 10.5 cm for the sensor antenna). This procedure can be repeated for other conditions such as different concrete thicknesses, concrete moisture and antenna sizes.

B. Wet Electrochemical Corrosion Cell

A wet electrochemical corrosion cell was employed to verify the operation of the sensor's potentiostat. In the wet electrochemical corrosion cell the electrodes are submerged in a liquid electrolyte, a 3% (weight per volume) NaCl solution in our case.

Linear polarization measurements were performed using the wet corrosion cell, the developed sensor and a benchtop precision potentiostat (VersaSTAT 3 from Princeton Applied Research). Figure 9 shows the linear polarization curve obtained with the benchtop potentiostat. The E_{OC} measured by the benchtop potentiostat is -643 mV. From the linear polarization curve in Figure 9 the polarization resistance R_p was estimated to be 0.75 kΩ.

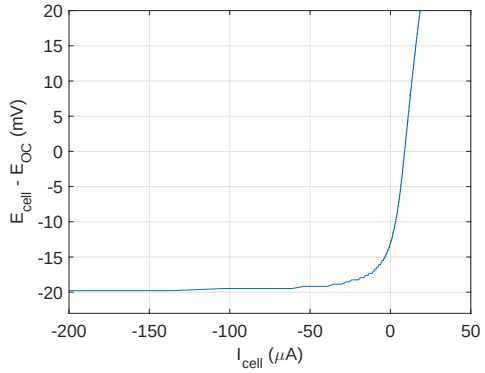

Figure 9. Linear polarization curve obtained using a benchtop potentiostat and a wet electrochemical corrosion cell.

A graphical user interface (GUI) that allows the user to issue commands to the sensor and read data from the sensor was developed. The GUI runs on a personal computer (PC) connected to the RFID reader through a serial port. If a CRC or a collision error is detected, the GUI automatically retries the last read/write operation assuring that the data collected from the sensor is free from transmission errors. Figure 10 shows the linear polarization curve obtained using the sensor and the developed GUI. The E_{OC} measured by the sensor's potentiostat is -645 mV, which is in good agreement with the E_{OC} read by the benchtop potentiostat.

As observed in Figure 10 the polarization curve from the sensor is somewhat noisy. Noise sources affecting the sensor's potentiostat include power supply noise due to finite isolation of the LDO regulator and induced noise from the field generated by the RFID reader. Although relatively small, the noise in the polarization curve can affect the calculation of the polarization resistance.

To remove the effect of noise, a cubic smoothing spline curve fitting was performed on the polarization curve [30]. The fitted curve is shown in Figure 10. Using the fitted polarization curve, the polarization resistance was estimated to be 0.71 kΩ,

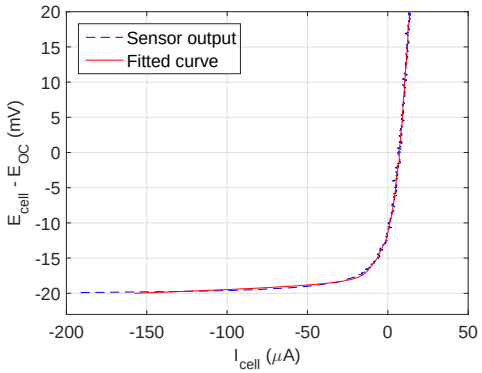

Figure 10. Linear polarization curve obtained using developed corrosion sensor and a wet electrochemical corrosion cell.

which is in good agreement with the value estimated from the polarization data collected with the benchtop potentiostat. The measurements performed with the wet corrosion cell validate the operation of the sensor's potentiostat and show that its performance is comparable to bulkier and more expensive solutions.

C. Concrete Corrosion Cell

Corrosion initiation in reinforced concrete structures typically occurs several years after deployment. In this work, an accelerated test was performed to assess the performance of the corrosion sensor in a concrete medium in a time span of days instead of several years. The test was performed using a concrete-based corrosion cell. The sensor's electrodes were embedded in a 5.7$\times$5.5$\times$2.5 cm^3 concrete sample. Pre-mixed concrete patch (Bondex from DAP) was used to prepare the concrete sample. The sample was allowed to cure for five days before collecting measurements. The sample was placed in a 3% (weight per volume) NaCl solution.

The small size of the concrete sample allows rapid diffusion of chloride ions to the working electrode initiating corrosion within days. Linear polarization measurements were performed on the concrete-based corrosion cell using the developed sensor and a benchtop potentiostat for 24 consecutive days. To perform measurements with the benchtop potentiosat, the sensor cover was removed, the electrodes disconnected from the PCB and connected to the benchtop potentiostat.

The acquired linear polarization curves were used to calculate the polarization resistance. Figure 11 shows the polarization resistance calculated using the polarization curves acquired with the benchtop potentiostat and with the developed RFID sensor. Notably, the data from the sensor and the benchtop potentiostat are in good agreement and show active corrosion by the day eight, which is marked by a large decrease in polarization resistance.

Figure 12 shows the OCP read by the sensor and the benchtop potentiostat. The figure also shows good agreement between both instruments. By day seven the OCP has fallen below -0.234 V indicating active corrosion (-0.234 V OCP measured with a silver/silver-chloride is equivalent to -0.350 V measured with a copper/copper sulfate electrode). Hence, according to the ASTM C 876 standard after day seven the

This article has been accepted for publication in a future issue of this journal, but has not been fully edited. Content may change prior to final publication. Citation information: DOI 10.1109/JSEN.2015.2476997, IEEE Sensors Journal

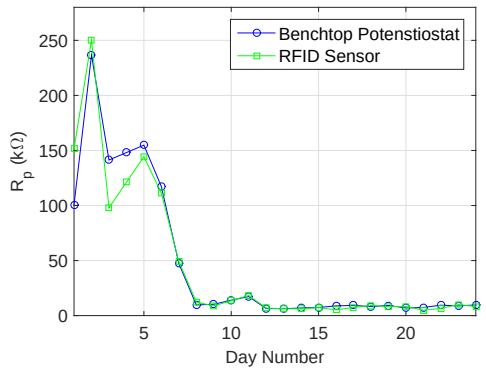

Figure 11. Calculated polarization resistance from linear polarization curves acquired with a benchtop potentiostat and the developed RFID sensor.

probability of corrosion is higher than 90%. After day 15, however, the OCP starts to increase steadily. When complemented with polarization resistance measurements, OCP readings give a more accurate picture of the corrosion process. Moreover, using the calculated polarization resistance values, and the accepted value of $B = 26$ mV for actively corroding steel, thickness reduction rate can be calculated using (7).

The developed sensor can also measure temperature. The effect of temperature on corrosion rate has been established in several studies [31]–[33]. The temperature information obtained from the sensor is intended to complement the OCP and linear polarization readings and provide a more complete understanding of the conditions leading to corrosion inside the concrete structure. The calibration and characterization of the temperature sensor is presented below. RFID communications between the reader and the sensor have been verified through a 6 cm concrete barrier.

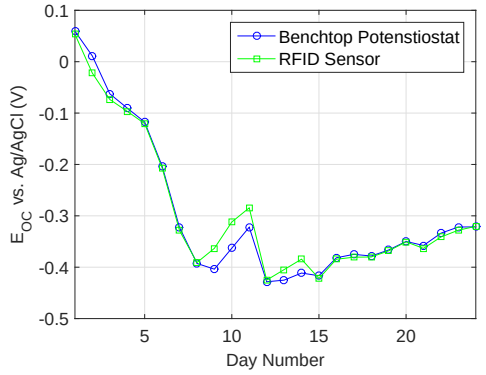

Figure 12. Measured OCP with a benchtop potentiostat and the developed RFID sensor.

D. Statistical Characterization of the Developed Sensor

The measurement uncertainty of the RFID corrosion sensor was evaluated following the statistical method described in the "Guide of Expression of Uncertainty in Measurement" (GUM) [34]. Repeated measurements of the OCP, temperature and cell current were performed with the RFID sensor and the concrete corrosion cell. From these measurements the mean and the standard uncertainty were calculated, where the standard uncertainty equals the standard deviation of the measurements [35].

Table II shows the mean ($\overline{E_{OC}}$) and the standard uncertainty (u_{OC}) of the OCP for 100 measurements taken with both the RFID sensor and the VersaSTAT benchtop potentiostat. A χ^2 goodness-of-fit test performed on the OCP readings indicates that the OCP readings are normally distributed at a significance level of 5%.

Table II
AVERAGE AND STANDARD UNCERTAINTY OF OCP MEASUREMENTS.

	RFID sensor	VersaSTAT
$\overline{E_{OC}}$ (V)	-0.321	-0.322
u_{OC} (V)	7.937×10^{-4}	7.886×10^{-4}
$\overline{E_{OC}} \pm K \cdot u_{OC}$	$[-0.3226, -0.3194]$ V	$[-0.3236, -0.3204]$ V

The table also shows the confidence interval $\overline{E_{OC}} \pm K \cdot u_{OC}$. In the table, a normal distribution for the OCP measurements and a coverage factor of $K = 2$ have been assumed for a 95% confidence interval. From the table it is seen that the confidence intervals of the RFID sensor and the VersaSTAT potentiostat are overlapping. Hence, the RFID sensor and the VersaSTAT potentionstat are said to be compatible when measuring the OCP [35].

The MSP430F2012 MCU employed in the RFID sensor has an on-chip temperature sensor connected to one of the MCU's internal ADC channels. A temperature read command has been implemented in the sensor's firmware. When this command is received from the reader, the MCU reads the output of its on-chip temperature sensor and stores the result in a pre-defined location in the EEPROM. The embedded temperature sensor has a linear response from -50 °C to 100 °C [36]. Hence, the relationship between the temperature sensor's output voltage, V_{temp}, and the temperature, T, can be expressed as:

$$T = G \times V_{temp} + T_{off} \tag{19}$$

where, G and T_{off} are the gain and the offset of the sensor. To calibrate the temperature sensor and find the values of G and T_{off}, temperature was measured at three different temperature points using the RFID sensor and the HH804U high-accuracy thermometer from OMEGA. Measurements were collected at room temperature, in a cold chamber with a nominal temperature of 4 (°C) and in a hot chamber with nominal temperature of 38 (°C). At each temperature point, 100 measurements were collected at an interval of one sample per second. A least-squares polynomial fit was employed with the average values of V_{temp} (from the sensor) and T (from the high-accuracy thermometer) to find the values of $G = 281.796$ °C/V and $T_{off} = -281.799$ °C.

Table III shows the average temperature ($\overline{T}$), the standard uncertainty (u_T) and the 95% confidence interval ($\overline{T} \pm K \cdot u_T$) for the HH804U high-accuracy thermometer and the calibrated temperature sensor. The overlapping confidence intervals indicate that the RFID sensor is compatible with the HH804U thermometer.

The uncertainty in the I_{cell} measurements can be evaluated by considering the current's path through the sensor's electronic circuitry. I_{cell} is converted to a voltage by the

This article has been accepted for publication in a future issue of this journal, but has not been fully edited. Content may change prior to final publication. Citation information: DOI 10.1109/JSEN.2015.2476997, IEEE Sensors Journal

Table III
AVERAGE AND STANDARD UNCERTAINTY OF TEMPERATURE MEASUREMENTS.

		$\overline{T}$ (°C)	u_T (°C)	$\overline{T} \pm K \cdot u_T$
Room temperature	RFID sensor	24.286	0.364	$[23.557, 25.014]$
	HH804U	24.332	0.124	$[24.084, 24.580]$
Cold chamber	RFID sensor	3.379	0.142	$[3.096, 3.662]$
	HH804U	3.664	0.063	$[3.538, 3.790]$
Hot chamber	RFID sensor	38.636	0.436	$[37.764, 39.509]$
	HH804U	38.228	0.155	$[37.918, 38.538]$

trans-impedance amplifier OA_2. The output of OA_2, V_{OA2}, is then quantized and converted to digital by the MCU's internal 10-bit ADC. The digital representation of V_{OA2} is then transmitted to the reader through the RFID inductive coupled link. At the reader, I_{cell} is recovered using:

$$I_{cell} = \frac{\widetilde{V}_{OA2} - V_{ref}}{R_{fb}} \tag{20}$$

where, $\widetilde{V}_{OA2}$ is the quantized version of V_{OA2}. Assuming uncorrelation between $\widetilde{V}_{OA2}$, V_{ref} and R_{fb} and applying the law of propagation uncertainty [34] to (20), results in the following expression for the combined standard uncertainty of I_{cell}:

$$u^2_{I_{cell}} = \frac{1}{R^2_{fb}} u^2_{\widetilde{V}_{OA2}} + \frac{1}{R^2_{fb}} u^2_{V_{ref}} + \left(\frac{V_{ref} - \widetilde{V}_{OA2}}{R^2_{fb}} \right)^2 u^2_{R_{fb}} \tag{21}$$

where, $u_{\widetilde{V}_{OA2}}$, $u_{V_{ref}}$ and $u_{R_{fb}}$ are the standard uncertainties of $\widetilde{V}_{OA2}$, V_{ref} and R_{fb} respectively. The values of the reference voltage and the feedback resistor were measured using a Fluke 179 multimeter resulting in $V_{ref} = 1.522$ V and $R_{fb} = 18.2$ kΩ. Given that the multimeter has a resolution of 0.001 V and 0.001 kΩ, and an accuracy of 0.09 % of reading + 2 counts for DC voltage measurements and 0.9 % of reading + 1 count for resistance measurements, the following confidence intervals are calculated: 1.522 ± 0.0021 V for V_{ref} and 18.2 ± 0.165 kΩ for R_{fb}. Assuming uniform distributions, we obtain the standard uncertainties: $u_{V_{ref}} = 0.0021/\sqrt{3} = 0.0012$ V and $u_{R_{fb}} = 0.165/\sqrt{3} = 0.095$ kΩ. The measured standard uncertainty of $\widetilde{V}_{OA2}$ is $u_{\widetilde{V}_{OA2}} = 4.643 \times 10^{-4}$ V.

Replacing values in (21) and considering $\widetilde{V}_{OA2} = 0$, the following I_{cell} standard uncertainty upper bound can be determined: $u_{I_{cell}} \leq 0.443$ μA. According to its manual, the VersaSTAT benchtop potentiostat has an current measurement accuracy of 0.2% of full scale. Hence, the standard uncertainty of the benchtop potentiostat is 0.231 μA (for a 200 μA scale and assuming a uniform distribution). The higher accuracy of the benchtop potentiostat is due to its superior shielding and higher resolution analog-to-digital conversion. However, its higher cost, size and power requirements preclude embedding it in concrete structures.

The standard uncertainty of the power supply measurements was also evaluated. To this end, 100 readings of the sensor's power supply voltage were acquired through the RFID interface resulting. The standard uncertainty of power supply voltage measurements was estimated to be 0.014 V.

The sensitivity of sensor's accuracy with respect to the circuit parameters R_{fb} and V_{ref} was evaluated using Monte Carlo simulations. Equation (21) was employed as the sensor's accuracy model. A variation of 10% around their nominal values was considered for R_{fb} and V_{ref}. The sensitivity was calculated using linear regression fitting on the results of the Monte Carlo simulations. The sensitivity of $u_{I_{cell}}$ with respect to R_{fb} was found to be -2.529×10^{-11} while the sensitivity of $u_{I_{cell}}$ with respect to V_{ref} was found to be 2.866×10^{-7}. Although small, the calculated sensitivities indicate that variations in the reference voltage V_{ref} have a greater impact on the standard uncertainty of the current cell measurements.

V. CONCLUSION

A RFID-based sensor suitable for corrosion monitoring in reinforced concrete structures has been presented. The sensor can perform linear polarization, open circuit potential and temperature measurements. The sensor obtains its power from an external RFID reader, which also functions as a datalogger. The sensor's electronic circuit comprises a RFID modem, a low-power microcontroller and a three-electrode low-power potentiostat. The proposed sensor can also measure its own power supply voltage and relay that information to the external reader which can then modify its power output accordingly. Communication between the sensor and the reader employ CRC and collision detection guaranteeing that the data read from the sensor is free from transmission errors. The measured power consumption of the sensor while performing a linear polarization measurement is 675 μW. The sensor's electronic circuit and the three electrodes are housed in a 3D-printed case measuring 11.8 cm×4 cm×5.6 cm. An accelerated corrosion test was conducted by embedding the encased sensor in concrete for 24 days. Linear polarization resistance measurements obtained from the embedded sensor show the initiation and progression of corrosion and are in good agreement with a much costlier and bulkier benchtop potentiostat. The proposed sensor can be installed in new structures before concrete is poured but it is also small enough to be installed in existing concrete structures via a back-filled core. The measurement accuracy of the proposed RFID-based sensor was characterized. It was found that the RFID-based sensor has a measurement accuracy comparable to precision benchtop instruments.

REFERENCES

[1] H.-W. Song and V. Saraswathy, "Corrosion monitoring of reinforced concrete structures - a review," *International Journal of Electrochemical Science*, vol. 2, pp. 1-28, 2007.

[2] G. H. Koch, M. Brongers, N. G. Thompson, Y. P. Virmani, and J. H. Payer, "Corrosion cost and preventive strategies in the United States," available online: https://www.nace.org/uploadedFiles/Publications/ccsupp.pdf, accessed on Jan. 2015, NACE, 2002.

[3] M. Yunovich, N. G. Thompson, T. Balvanyos, and L. Lave, "Corrosion cost and preventive strategies in the United States, Appendix D, highway bridges", available online: http://www.dnvusa.com/Binaries/highway_tcm153-378806.pdf, accessed on Jan. 2015, Federal Highway Administration, 2001.

[4] M. Andringa, D. Keikirk, N. Dickerson and S. Wood, "Unpowered wireless corrosion sensor for steel reinforced concrete," *IEEE Sensors*, 2005.
[5] A. A. Yousef, "Resonant sensors for detecting corrosion in concrete bridges," *Transportation Research Record: Journal of the Transportation Research Board*, vol. 2201, no. 1, pp. 19-26, 2010.
[6] M. M. Andringa, J. M. Puryear, D. P. Neikirk and S. L. Wood, "Low-cost wireless corrosion and conductivity sensors," *Proceedings of the SPIE - The International Society for Optical Engineering*, vol. 6174, pp. 61740X-1-61740X-8, 2006.
[7] D. G. Water, O. Jayaweera, A. J. Bahr, D. L. Huestis, N. Priyanhta, R. Meline, R. Reis and D. Parks, "Smart Pebble: wireless sensor for structural health monitoring of bridge decks,: *Proceedings of the SPIE*, vol. 5057, no. 20, 2003.
[8] K. Perveen, G. E. Bridges, S. Bhadra and D. J. Thomson, "Corrosion potential sensor for remote monitoring of civil structure based on printed circuit board sensor," *IEEE Transactions on Instrumentation and Measurement*, vol. 63, no. 10, Oct. 2014.
[9] S. Bhadra, D. J. Thomson and G. E. Bridges, "A wireless embedded passive sensor for monitoring the corrosion potential of reinforcing steel," *Smart Materials and Structures*, vol. 22, no. 7, 2013.
[10] M. Alamin, G. Y. Tian, A. Andrews and P. Jackson, "Corrosion detection using low-frequency RFID technology," *Insight-Non-Destructive Testing and Condition Monitoring*, vol. 54, no. 2, pp. 72-75, 2012.
[11] H. Zhang, G. Y. Tian, A. Simm and M. Alamin, "Electromagnetic methods for corrosion under paint coating measurement," *International Symposium on Precision Engineering Measurement and Instrumentation*, pp. 875919-1-8759-10, 2012.
[12] J. P. Broomfield, J. Rodriguez, L. M. Ortega, and A. M. Garcia. "Techniques to assess the corrosion activity of steel reinforced concrete structures." *ASTM STP 1276*, pp. 91-106, 1996.
[13] Virginia Technologies, Inc. [Online]. Available at: http://corrosioninstrument.com/, accessed on Jan. 2015.
[14] W. Leon-Salas, S. Kanneganti and C. Halmen, "Development of a smart RFID-based corrosion sensor," *IEEE Sensors*, pp. 534-537, 2011.
[15] C. Andrade and C. Alonso, "On-site measurements of corrosion rate of reinforcements," *Construction and Building Materials*, vol. 15, no, 2, pp. 141-145, 2001.
[16] C. Alonso, C. Andrade, X. R. Nóvoa, M. Izquierdo and M. C. Pérez, "Effect of protective oxide scales in the macrogalvanic behaviour of concrete reinforcements," *Corrosion Science*, vol. 40, no. 8, pp. 1379-1389, 1998.
[17] S. Ahmad, "Reinforcement corrosion in concrete structures, its monitoring and service life prediction - a review," *Cement and Concrete Composites*, vol. 25, no. 4, pp. 459-471, 2003.
[18] M. F. Montemor, A. M. P. Simões and M. G. S. Ferreira, "Chloride-induced corrosion on reinforcing steel: from the fundamentals to the monitoring techniques," *Cement and Concrete Composites*, vol. 25, pp. 491-502, 2003.
[19] Mansfeld, Florian and Kendig, MW and Tsai, S, "Recording and analysis of AC impedance data for corrosion studies," *Corrosion*, vol. 38, no. 11, pp. 570-580, 1982.
[20] P. Roberge, *Corrosion Engineering: Principles and Practices*, first edition, McGraw Hill, 2008/
[21] B. Elsener, C. Andrade, J. Gulikers, R. Polder, M. Raupach, "Hall-cell potential measurements - Potential mapping on reinforced concrete structures," *Materials and Structures*, vol. 36, no. 7, pp. 461-471, 2003.
[22] M. Stern and A. Geary, "Electrochemical polarization I. A theoretical analysis of the shape of polarization curves," *Journal of the Electrochemical Society*, vol. 104, no. 1, pp. 56-63, 1957.
[23] M. Stern, "A method for determining corrosion rates from linear polarization data," *Corrosion*, vol. 14, 1958.
[24] C. Andrade and J. A. Gonzalez, "Quantitative measurements of corrosion rate of reinforcing steels embedded in concrete using polarization resistance measurements," *Materials and Corrosion*, vol. 29, no. 8, pp. 515-519, 1978.
[25] J. R. Scully, "Polarization resistance method for determination of instantaneous corrosion rates," *Corrosion*, vol. 56, no. 2, pp. 199-218, 2000.
[26] E. Bardal (Ed.), *Corrosion and Protection*, Springer Science & Business Media, 2004.
[27] K. Van Schuylenbergh and R. Puers, *Inductive Powering: Basic Theory and Application to Biomedical Systems*, Springer, 2009.
[28] Cathodic Protection Co., *Permanent Ag/AgCl reference electrode*, Available online: http://www.refcells.com/pdfs/AG4.pdf, Accessed Feb. 2015.
[29] K. Finkenzeller, *RFID Handbook*, 3rd edition, Wiley, 2012.
[30] P. Craven and G. Wahba, "Smoothing noisy data with spline functions," *Numerischel Mathematik*, vol. 31, no. 4, pp. 377-403, 1979.
[31] M. Pour-Ghaz, O. B. Isgor and P. Ghods, "The effect of temperature on the corrosion of steel in concrete. Part 1: Simulated polarization resistance test and model development," *Corrosion Science*, vol. 51, no. 2, pp. 415-425, 2009.
[32] J. M. Deus, B. Díaz, L. Freire, X. R. Nóvoa, "The electrochemical behaviour of steel rebars in concrete: an Electrochemical Impedance Spectroscopy study of the effect of temperature," *Electrochimica Acta*, vol. 131, no. 10, pp. 106-115, 2014.
[33] J. Hu, X. Cheng, X. Li, P. Deng and G. Wang, "The coupled effect of temperature and carbonation on the corrosion of rebars in the simulated concrete pore solutions," *Journal of Chemistry*, vol. 2015, Article ID 462605, 6 pages, 2015. doi:10.1155/2015/462605.
[34] "Guide to the expression of uncertainty in measurement," BIPM, IEC, IFCC, ISO, IUPAC and OIML, 1993.
[35] A. Ferrero and S. Salicone, "Measurement uncertainty," *IEEE Instrumentation and Measurement Magazine*, vol. 9, no. 3, pp. 44-51, 2006.
[36] Texas Instruments, *MSP430x2xx Family User's Guide*, Available online: http://www.ti.com/lit/ug/slau144j/slau144j.pdf, Accessed June, 2015.